

Effect of initial volume fraction on the collapse of granular columns in fluid

K. Kumar

Computational Geomechanics Research Group, Department of Engineering, University of Cambridge, UK

J-Y. Delenne

IATE, UMR 1208 INRA-CIRAD-Montpellier Supagro-UM2, University of Montpellier 2, France.

K. Soga

Department of Civil and Environmental Engineering, University of California, Berkeley, USA.

ABSTRACT: This paper investigates the effect of initial volume fraction on the runout characteristics of granular column collapse in a fluid. Two-dimensional sub-grain scale numerical simulations are performed to understand the flow dynamics of granular collapse in a fluid. The Discrete Element (DEM) technique is coupled with the Lattice Boltzmann Method (LBM), for fluid-grain interactions, to understand the evolution of submerged granular flows. The fluid phase is simulated using Multiple-Relaxation-Time LBM (LBM-MRT) for numerical stability. In order to simulate interconnected pore space in 2D, a reduction in the radius of the grains (hydrodynamic radius) is assumed during LBM computations. A parametric analysis is performed to assess the influence of the granular characteristics (initial packing) on the evolution of flow and run-out distances. The volume of the initial packing is changed to simulate different stress conditions while maintaining the same aspect ratio. The influence of the stress condition on the run-out behaviour is studied for different permeabilities. The granular flow dynamics is investigated by analysing the effect of hydroplaning, water entrainment and viscous drag on the granular mass. The mechanism of energy dissipation, the shape of the flow front, water entrainment and evolution of packing density is used to explain the difference in the flow characteristics of loose and dense granular column collapse in a fluid.

1 INTRODUCTION

The flow of dense granular material is a common phenomenon in engineering predictions, such as avalanches, landslides, and debris-flow modelling. Despite the huge amount of research that has gone into describing the behaviour of granular flows, a constitutive equation that describes the overall behaviour of a flowing granular material is still lacking. The initiation and propagation of submarine granular flows depend mainly on the slope, density, and quantity of the material destabilised. Although certain macroscopic models are able to capture the simple mechanical behaviours, the complex physical mechanisms that occur at the grain scale, such as hydrodynamic instabilities, the formation of clusters, collapse, and transport, have largely been ignored (Topin et al. 2011). The momentum transfer between the discrete and the continuous phases significantly affects the dynamics of the flow (Peker and Helvacı 2007). Grain-scale description of the granular material enriches the

macro-scale variables, which poorly account for the local rheology of the materials. In order to describe the mechanism of saturated and/or immersed granular flows, it is important to consider both the dynamics of the solid phase and the role of the ambient fluid (Denlinger and Iverson 2001). In particular, when the solid phase reaches a high volume fraction, it is important to consider the strong heterogeneity arising from the contact forces between the grains, the drag interactions which counteract the movement of the grains, and the hydrodynamic forces that reduce the weight of the solids inducing a transition from dense compacted to a dense suspended flow (Meruane et al. 2010). The case of the collapse in presence of an interstitial fluid has been less studied. In this paper, we study the submarine granular flows in the inclined configuration. We study the effect of permeability, density and slope angle on the run-out evolution.

2 LBM FORMULATION

The Lattice Boltzmann Method is a ‘micro-particle’ based numerical time-stepping procedure for the solution of incompressible fluid flows. Consider a 2D incompressible fluid flow with density ρ and kinematic viscosity ν , in a rectangular domain D . The fluid domain is divided into a rectangular grid or lattice, with the same spacing ‘ h ’ in both the x - and the y -directions, as shown in figure 1. The present study focuses on two-dimensional problems, hence the $D2Q9$ momentum discretisation is adopted (see He et al. (1997) for naming convention).

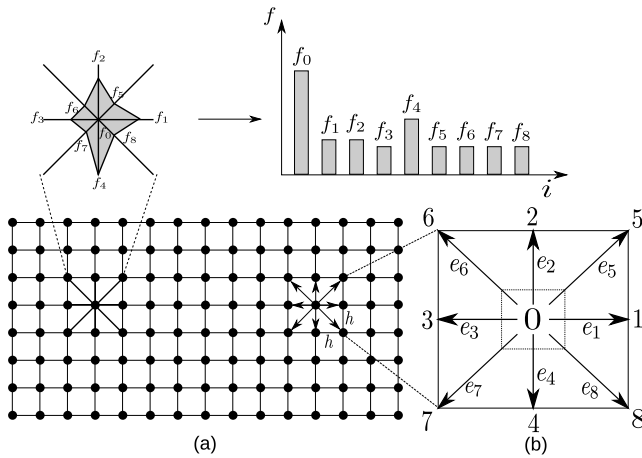


Figure 1: The Lattice Boltzmann discretisation and D2Q9 scheme: (a) a standard LB lattice and histogram views of the discrete single particle distribution function/direction-specific densities f_i ; (b) D2Q9 model

The lattice Boltzmann Bhatnagar-Gross-Krook (LGBK) method is capable of simulating various hydrodynamics (Succi 2001) and offers intrinsic parallelism. Although LBM is successful in modelling complex fluid systems, such as multiphase flows and suspensions in fluid, the LBM may lead to numerical instability when the dimensionless relaxation time τ is close to 0.5. The Multi-Relaxation Time Lattice Boltzmann Method (LBM-MRT) overcomes the deficiencies of linearised single relaxation LBM-BGK, such as fixed Prandtl number ($Pr=\nu/\kappa$), where the thermal conductivity ‘ κ ’ is unity (Liu et al. 2003). The LB-MRT model offers better numerical stability and has more degrees of freedom. In the formulation of the linear Boltzmann equation with multiple relaxation time approximation, the lattice Boltzmann equation is written as:

$$f_\alpha(\mathbf{x} + \mathbf{e}_i \Delta t, t + \Delta t) - f_\alpha(\mathbf{x}, t) = -\mathbf{S}_{\alpha i}(f_i(\mathbf{x}, t) - f_i^{eq}(\mathbf{x}, t)) \quad (1)$$

where \mathbf{S} is collision matrix. The nine eigen values of \mathbf{S} are all between 0 and 2 so as to maintain linear stability and the separation of scales, which means that the relaxation times of non-conserved quantities are much faster than the hydrodynamic time scales. The

LGBK model is the special case in which the nine relaxation times are all equal and the collision matrix $\mathbf{S} = \frac{1}{\tau} \mathbf{I}$, where \mathbf{I} is the identity matrix. The evolutionary progress involves two steps, advection and flux. The advection can be mapped to the momentum space by multiplying through by a transformation matrix \mathbf{M} and the flux is still finished in the velocity space. The evolutionary equation of the multi-relaxation time lattice Boltzmann equation is written as:

$$\begin{aligned} & \mathbf{f}(\mathbf{x} + \mathbf{e}_i \Delta t, t + \Delta t) - \mathbf{f}(\mathbf{x}, t) \\ &= -M^{-1} \hat{\mathbf{S}}(\hat{\mathbf{f}}(\mathbf{x}, t) - \hat{\mathbf{f}}^{eq}(\mathbf{x}, t)) \end{aligned} \quad (2)$$

where \mathbf{M} is the transformation matrix mapping a vector \mathbf{f} in the discrete velocity space $V = R^b$ to a vector $\hat{\mathbf{f}}$ in the moment space $V = R^b$.

$$\hat{\mathbf{f}} = \mathbf{M}\mathbf{f} \quad (3)$$

$$\mathbf{f}(\mathbf{x}, t) = [f_0(\mathbf{x}, t), f_1(\mathbf{x}, t), \dots, f_8(\mathbf{x}, t)]^T \quad (4)$$

The collision matrix $\hat{\mathbf{S}} = M S M^{-1}$ in moment space is a diagonal matrix: $\hat{\mathbf{S}} = \text{diag}[s_1, s_2, s_3, \dots, s_9]$. The transformation matrix \mathbf{M} can be constructed via Gram-Schmidt orthogonalisation procedure. Through the Chapman-Enskog expansion (Du et al. 2006), the incompressible Navier-Stokes equation can be recovered and the viscosity is given as:

$$\nu = c_s^2 \Delta t (\tau - 0.5) \quad (5)$$

2.1 Turbulence in Lattice Boltzmann Method

Modelling fluids with low viscosity like water remains a challenge, necessitating very small values of h , and/or τ very close to 0.5 (He et al. 1997). Turbulent flows are characterised by the occurrence of eddies with multiple scales in space, time and energy. In this study, the Large Eddy Simulation (LES) is adopted to solve for turbulent flow problems. The separation of scales is achieved by filtering of the Navier-Stokes equations, from which the resolved scales are directly obtained and unresolved scales are modelled by a one-parameter Smagorinski sub-grid methodology, which assumes that the Reynold’s stress tensor is dependent only on the local strain rate (Smagorinsky 1963). The turbulent viscosity ν is related to the strain rate S_{ij} and a filtered length scale ‘ h ’ as follows:

$$v_t = (S_c h)^2 \bar{S}; \quad (6)$$

$$\bar{S} = \sqrt{\sum_{i,j} \tilde{S}_{i,j} \tilde{S}_{i,j}} \quad (7)$$

where S_c is the Smagorinski constant found to be close to 0.03 (Yu et al. 2005).

The effect of the unresolved scale motion is taken into account by introducing an effective collision relaxation time scale τ_t , so that the total relaxation time τ_* is written as:

$$\tau_* = \tau + \tau_t \quad (8)$$

where τ and τ_t are respectively the standard relaxation times corresponding to the true fluid viscosity ν and the turbulence viscosity ν_t , defined by a sub-grid turbulence model. The new viscosity ν_* corresponding to τ_* is defined as:

$$\nu_* = \nu + \nu_t = \frac{1}{3}(\tau + \tau_t - \frac{1}{2})C^2\Delta t \quad (9)$$

$$\nu_t = \frac{1}{3}\tau_t C^2\Delta t \quad (10)$$

The Smagorinski model is easy to implement and the Lattice Boltzmann formulation remains unchanged, except for the use of a new turbulence-related viscosity τ_* . The component s_1 of the collision matrix becomes $s_1 = \frac{1}{\tau + \tau_t}$.

3 COUPLED LB - DEM FOR FLUID-PARTICLE INTERACTIONS

The Lattice Boltzmann approach has the advantage of accommodating large particle sizes and the interaction between the fluid and the moving particles can be modelled through relatively simple fluid - particle interface treatments. Further, employing the Discrete Element Method (DE) to account for the particle/particle interaction naturally leads to a combined LB - DEM solution procedure. The Eulerian nature of the Lattice Boltzmann formulation, together with the common explicit time step scheme of both the Lattice Boltzmann and the Discrete Element makes this coupling strategy an efficient numerical procedure for the simulation of particle-fluid systems (Cook et al. 2004). In order to capture the actual physical behaviour of the fluid-particle system, the boundary condition between the fluid and the particle is modelled as a non-slip boundary condition, i.e. the fluid near the particle should have similar velocity as the particle boundary. The solid particles inside the fluid are represented by lattice nodes. The discrete nature of lattice will result in stepwise representation of the surfaces. Very small lattice spacing is adopted to obtain smoother boundaries.

4 UNDERWATER GRANULAR FLOWS

In this study, a 2D poly-disperse system ($d_{max}/d_{min} = 1.8$) of circular discs in fluid was used to understand the behaviour of granular flows on inclined planes (see Figure 2). The soil column was modelled using 1000 discs of density 2650 kg m^{-3}

and a contact friction angle of 26° . The collapse of the column was simulated inside a fluid with a density of 1000 kg m^{-3} and a kinematic viscosity of $1 \times 10^{-6} \text{ m}^2 \text{ s}^{-1}$. The choice of a 2D geometry has the advantage of cheaper computational effort than a 3D case, making it feasible to simulate very large systems. A granular column of aspect ratio ‘a’ of 0.8 was used. Dry analyses were also performed to study the effect of hydrodynamic forces on the run-out distance.

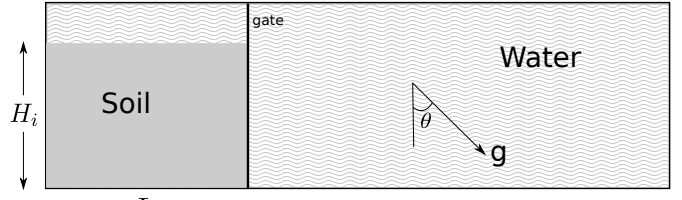


Figure 2: Underwater granular collapse set-up

4.1 Effect of initial packing density

Rondon, Pouliquen, & Aussillous 2011 observed that the loose packings flow rapidly on a time scale proportional to the initial height and results in longer run-out distance in comparison to the dense packing. Hydroplaning occurs above a critical Froude’s number of 0.4. The Froude’s number is inversely related to the thickness of the flow and its density. Hence, for the same thickness of flow, a loose granular column will experience more hydroplaning than a dense granular flow. This effect might result in longer run-out behaviour in fluid than the dry condition for the same initial aspect ratio. The initial packing density and the permeability of a 2D granular column, with an aspect ratio of 0.8, are varied to understand their influence on the run-out behaviour. The run-out behaviour of the dense case (83% packing density), is compared with a loose granular column (79% packing fraction). The permeability is varied by changing the hydrodynamic radius from $0.7 R$ to $0.95 R$.

The normalised run-out for different hydrodynamic radii for a granular column with an initial aspect ratio of 0.8 for dense initial packing are presented in figure 3. The run-out increases with decrease in the permeability, which is equivalent to an increase in the hydrodynamic radius. An increase in the hydrodynamic radius from 0.7 to $0.95 R$ increases the normalised run-out by 25%. However, even under a very low permeability condition ($r = 0.95 R$), the run-out observed in fluid is shorter than the dry and the buoyant conditions.

At a high permeability ($r = 0.7 R$), the evolution of run-out at the initial stage is quicker, which means that the negative pore-pressure that is developed during the shearing along the shear-failure surface is dissipated faster. Even though the negative pore-pressure is dissipated, due to the development of negative pore-pressure the evolution of run-out in fluid is slower

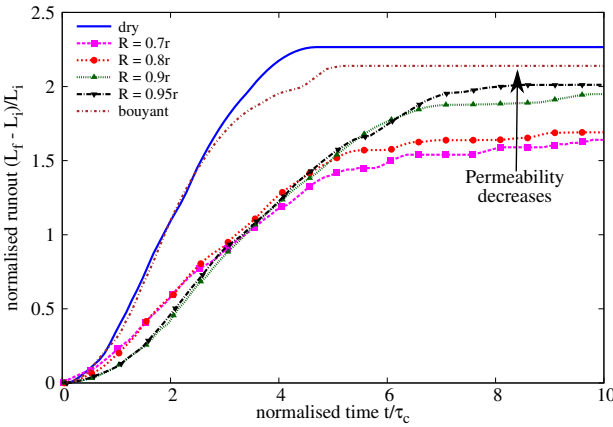
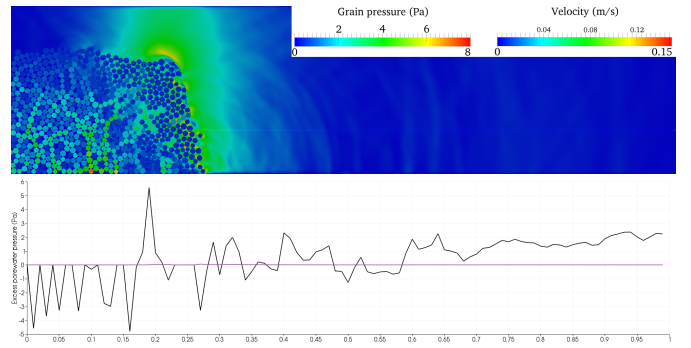


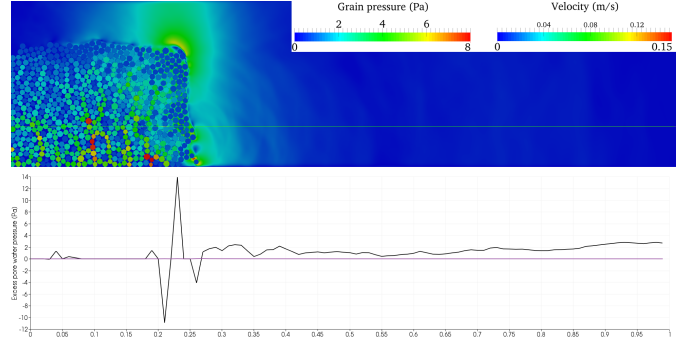
Figure 3: Effect of permeability on the evolution of run-out for a column collapse in fluid ($a = 0.8$).

than its dry counterpart. The rate of pore-pressure dissipation decreases with decrease in the permeability. This can be observed by a flatter slope in the run-out evolution with decrease in the permeability. Figure 4 shows the distribution of pore-pressure in high and low permeability granular media along the horizontal direction at a height of $10 \times d$ from the base. In LBM, the pore-pressure in fluid is a function of fluid density distribution functions. At time $t = \tau_c$, the highly permeable ($r = 0.7 R$) granular column shows smaller negative pore-pressure in comparison to large negative pore-pressures observed in the shearing zone of a low permeable column ($r = 0.9 R$). This shows that not only does it take longer for the pore-pressure to dissipate with a decrease in permeability, but also results in almost twice the negative pore-pressure than what is observed in the high permeable case (figures 4b and 4d). A high value of positive pore-pressure is observed at the face of the column in the low permeable condition. This indicates that the low permeable column fails as a continuous block undergoing a shear failure, which generates a very large negative pore-pressure along the failure surface. However, in the case of the high permeable column the failure is more localised with multiple negative pore-pressure spikes (figure 4c).

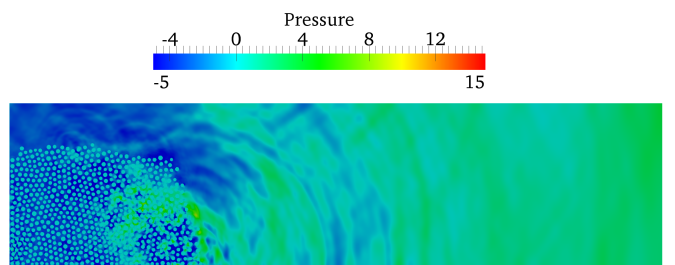
Although the low permeability granular columns require a longer duration for the run-out to evolve, the final run-out distance is found to be much longer than in the high permeable condition. Figure 5 shows that the potential energy mobilised during the flow of a low permeability column is 20% smaller than the collapse of a high permeability granular column. Normalised kinetic energy evolution with time (figure 6) shows that the low permeability column has a wider peak kinetic energy distribution in comparison to a sharp peak observed in the high permeability condition. This indicates the influence of lubrication, i.e., hydroplaning of the granular flow in low permeability conditions. The evolution of the horizontal kinetic energy with time reveals that the peak kinetic energy is sustained longer as the permeability of the granular material decreases (figure 6b). Although the peak kinetic energy is smaller in the low permeability case,



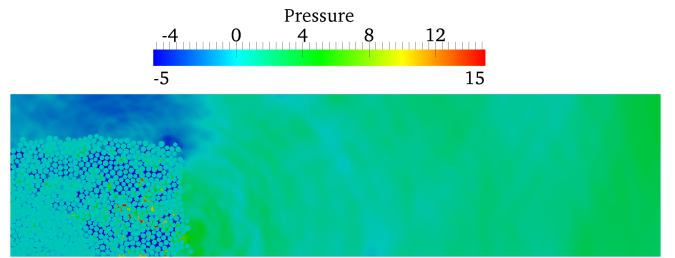
(a) High permeability ($r = 0.7 R$) - Pressure at the bottom of the granular flow.



(b) Low permeability ($r = 0.95 R$) - Pressure at the bottom of the granular flow.



(c) High permeability ($r = 0.7 R$) - Pressure contour (Pa).



(d) Low permeability ($r = 0.95 R$) - Pressure contour (Pa).

Figure 4: Effect of permeability on the excess pore water pressure distribution for a granular column collapse in fluid ($a = 0.8$ & dense packing) at $t = \tau_c$ along the horizontal direction at a height of $10d$ from the base.

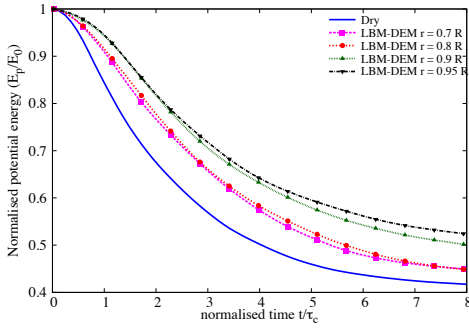
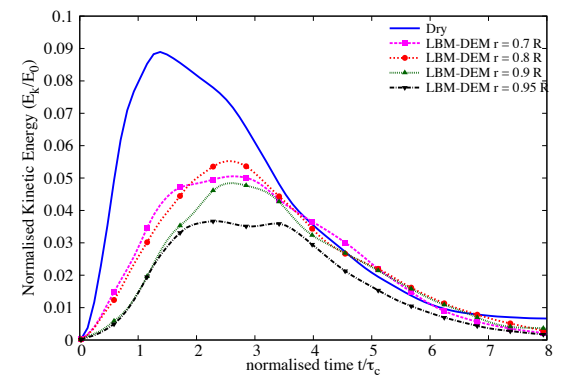


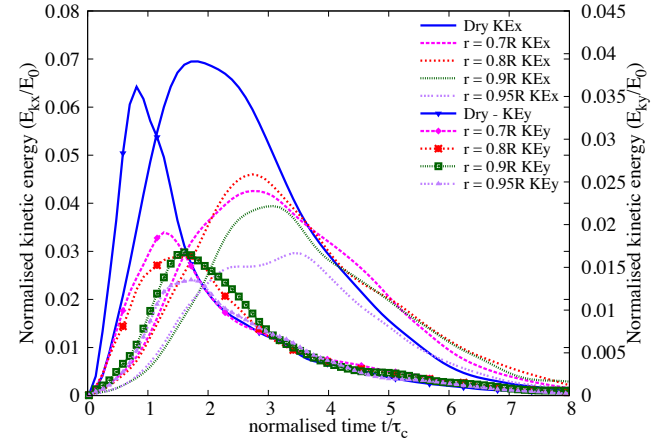
Figure 5: Effect of permeability on the evolution of the potential energy with time for a granular column collapse in fluid ($a = 0.8$).

the hydroplaning of the flowing granular mass results in a longer run-out distance. Figures 7b and 7d shows the distribution of pore-pressure for a dense granular column collapse in fluid along the bottom plane. A high positive pore-pressure is observed at the base of the granular flow at the flow front in low permeability condition indicating the occurrence of hydroplaning. The positive pore-pressure at the flow front decreases the effective stress thus the creating lubrication effect. The evolution of local packing density with time shows that the packing density decreases with decrease in permeability (figure 8a). This drop in the value of packing density between $t = 2\tau_c$ and $t = 3\tau_c$ corroborates with the duration of hydroplaning during which a large amount of water is entrained at the flow front.

The high permeability granular column shows lower water entrainment (figure 8a), which indicates that for highly permeable flows the drag force acting on the soil grains predominates over the lubrication effect on the run-out behaviour. Figure 8b shows the evolution of Froude's number with time for different permeability conditions. In dense granular columns, the Froude's number increases with decrease in permeability, however the Froude's number is below a critical value of 0.4 even for a low permeable column. Hence, no hydroplaning is observed. In both the low and high permeable granular flows, the granular material consolidates at the final stage of the flow (figure 8a). This can be observed by the increase in the packing density at the final stage due to settlement of grains and expulsion of entrained water. The final deposit profile for both low and high permeability conditions are shown in ???. The high permeability collapse shows a more parabolic (convex) deposit profile in contrast to the more concave profile observed in the low permeability condition. In high permeable condition, once the granular mass is mobilised, the drag forces slows down the rate of flow, which allows the grains to densify resulting in a more parabolic profile. This is in contrast to the hydroplaning observed in the low permeability condition, where the granular mass thickness is smaller than the dense condition. The observation of hydroplaning in the low permeable condition may be due to the difference in the distribution of granular mass at the flow front.

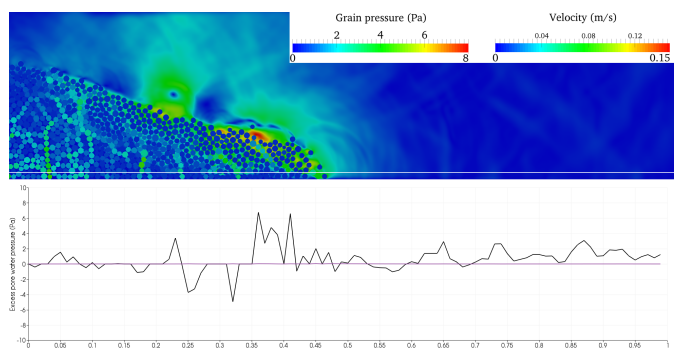


(a) Evolution of the total kinetic energy.

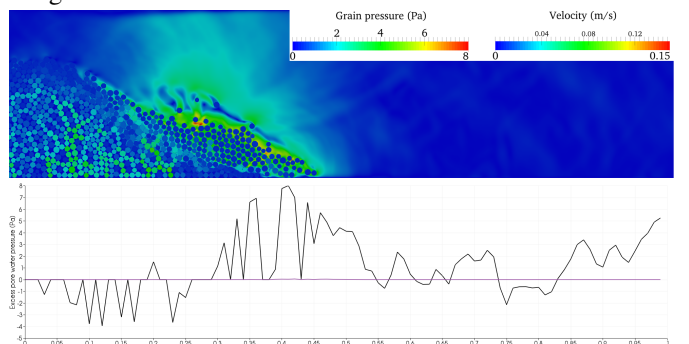


(b) Evolution of horizontal and vertical kinetic energies.

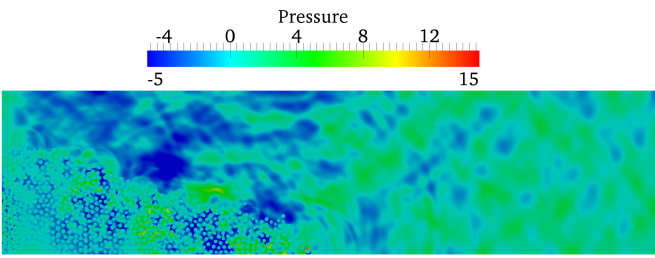
Figure 6: Effect of permeability on the evolution of kinetic energies with time for a granular column collapse in fluid ($a = 0.8$).



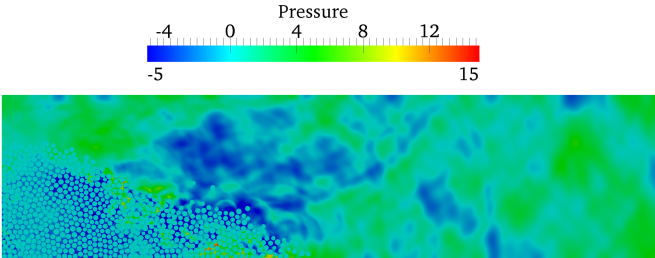
(a) High permeability ($r = 0.7 R$) - Pressure at the bottom of the granular flow.



(b) Low permeability ($r = 0.95 R$) - Pressure at the bottom of the granular flow.



(c) High permeability ($r = 0.7 R$) - Pressure contour (Pa).



(d) Low permeability ($r = 0.95 R$) - Pressure contour (Pa).

Figure 7: Effect of permeability on the excess pore water pressure distribution along the bottom plane for a granular column collapse in fluid ($a = 0.8$ & dense packing) at $t = 2\tau_c$.

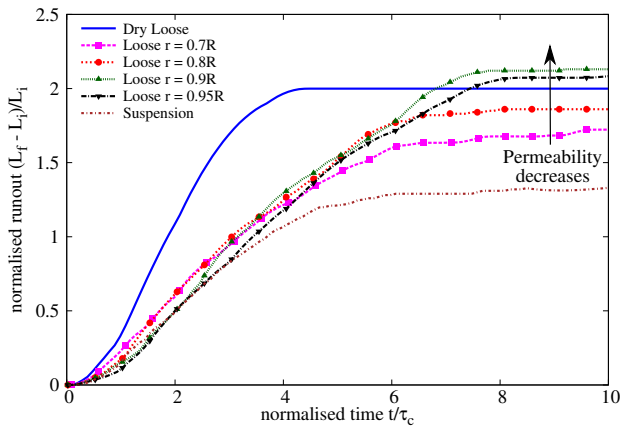
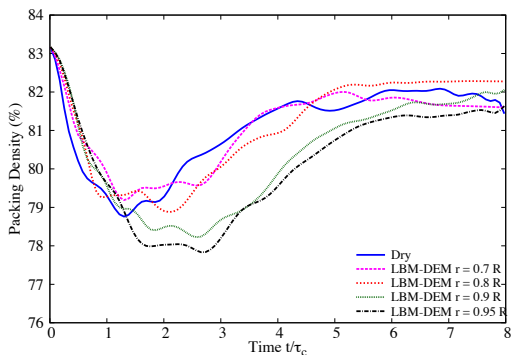


Figure 9: Effect of permeability on the evolution of run-out for a column collapse in fluid ($a = 0.8$ & loose packing).

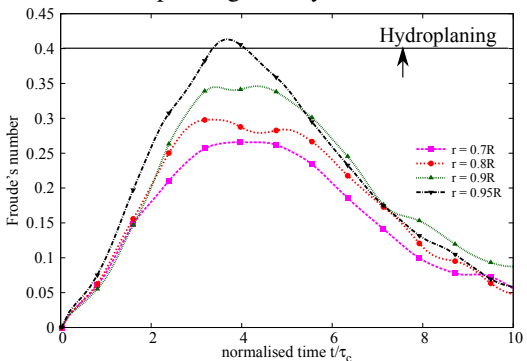
The normalised run-out evolution with time for a loose initial packing (79% packing fraction) with different hydrodynamic radii $0.7 R$, $0.8 R$, 0.9 and $0.95 R$ are presented in figure 9. The run-out evolution a column of grains in suspension is compared with the dry and submerged granular columns to understand the influence of hydrodynamic forces on the flow kinematics. Similar to the dense granular column, the run-out distance increases with increase in the hydrodynamic radius (i.e., decrease in permeability). At low permeabilities ($r = 0.9$ and $0.95 R$), the run-out distance is longer than the dry condition. This shows that the lubrication effect in low permeability conditions overcomes the influence of the drag force and the development of large negative pore-pressure resulting in a longer run-out distance. Although the suspended granular masses experience higher drag forces and turbulent effects, the run-out evolves almost at the same rate in comparison with granular columns with high permeability. This shows the effect of permeability on the dissipation rate of negative pore-pressure developed during the initial stage of collapse.

Figure 10 shows the development of negative pore-pressure in low permeability ($r = 0.95 R$) and dissipation of negative pore-pressure in high permeability ($r = 0.7 R$) at the same time $t = \tau_c$. This difference in the quantity and the rate of dissipation of negative pore-pressure results in a difference in the rate of flow evolution. A low permeability column requires a longer duration to evolve. Figure 11 shows the distribution of the excess pore-pressure along the bottom for low and high permeability conditions. As the flow progresses, the low permeability of the granular column causes hydroplaning to occur at the base of the column, which can be observed by high positive pore-pressure at the base of the flow front (figures 11b and 11d), resulting in a longer run-out distance.

The evolution of the potential energy with time (figure 12) reveals that at a very low permeability ($r = 0.95 R$), the initial potential energy mobilised is smaller than at $r = 0.9 R$. Also with decreasing permeability, the time required to dissipate the negative pore-pressure increases. This results in a shorter run-out distance in the case of $r = 0.95 R$ to that of $r = 0.9$

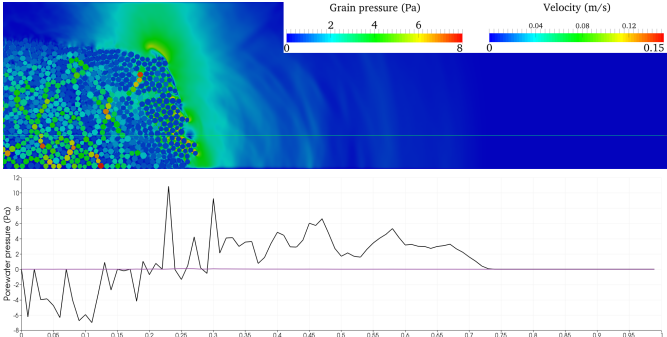


(a) Evolution of the packing density.

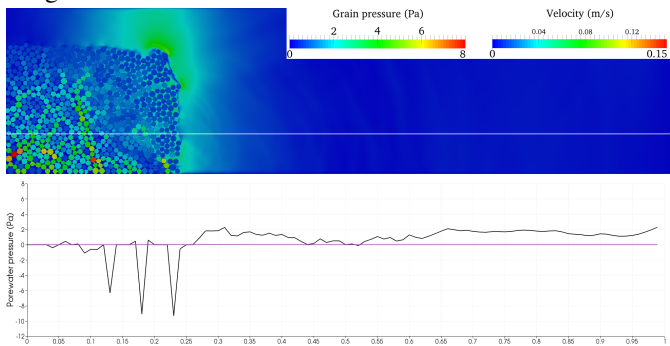


(b) Evolution of the Froude's number.

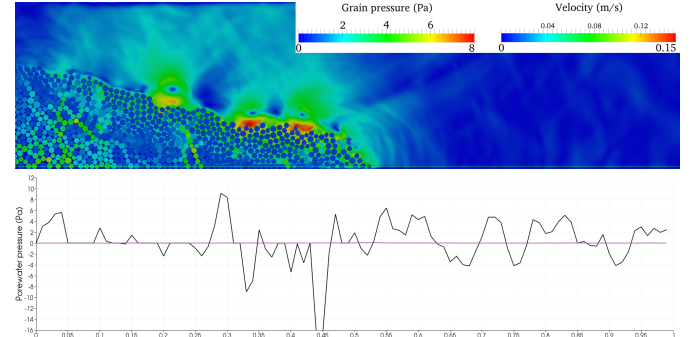
Figure 8: Effect of permeability on the evolution of packing density and Froude's number for a granular column collapse in fluid ($a = 0.8$ & dense initial packing).



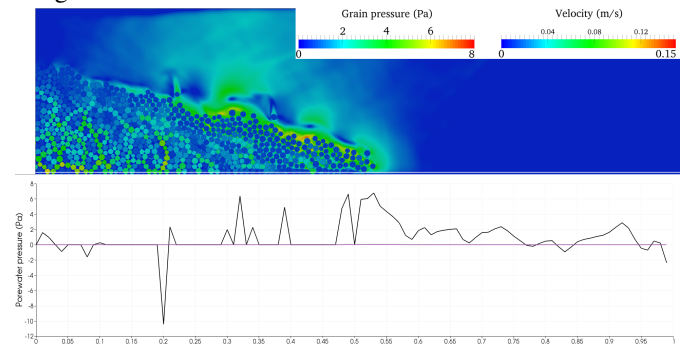
(a) High permeability ($r = 0.7 R$) - Pressure at the bottom of the granular flow.



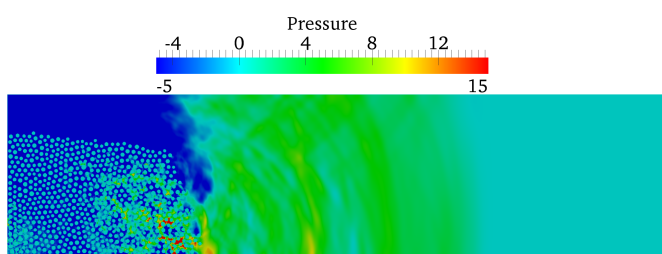
(b) Low permeability ($r = 0.95 R$) - Pressure at the bottom of the granular flow.



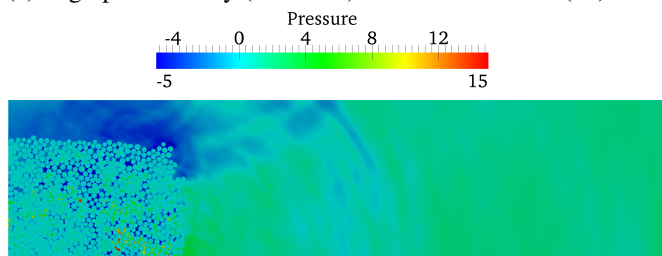
(a) High permeability ($r = 0.7 R$) - Pressure at the bottom of the granular flow.



(b) Low permeability ($r = 0.95 R$) - Pressure at the bottom of the granular flow.

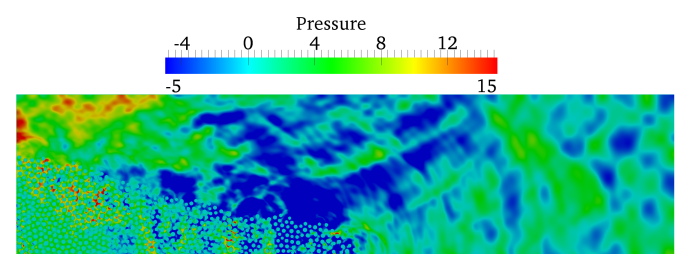


(c) High permeability ($r = 0.7 R$) - Pressure contour (Pa).

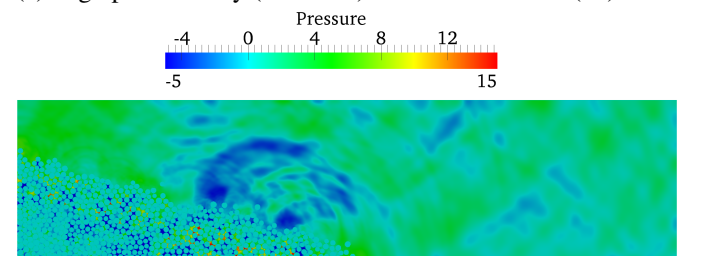


(d) Low permeability ($r = 0.95 R$) - Pressure contour (Pa).

Figure 10: Effect of permeability on the excess pore water pressure distribution along the base of a granular column collapse in fluid ($a = 0.8$ & loose packing) at $t = \tau_c$.



(c) High permeability ($r = 0.7 R$) - Pressure contour (Pa).



(d) Low permeability ($r = 0.95 R$) - Pressure contour (Pa).

Figure 11: Effect of permeability on the excess pore water pressure distribution for a granular column collapse in fluid ($a = 0.8$ & loose packing) at $t = 2\tau_c$.

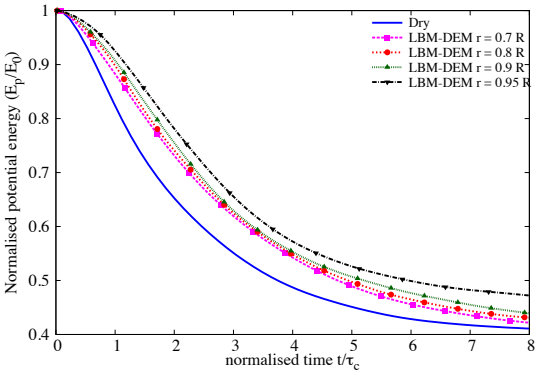
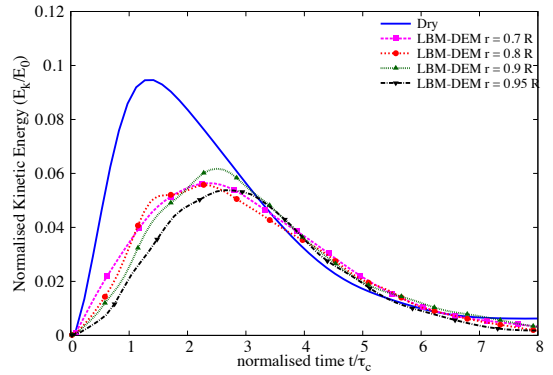


Figure 12: Effect of permeability on the evolution of the potential energy with time for a granular column collapse in fluid ($a = 0.8$ & loose packing).

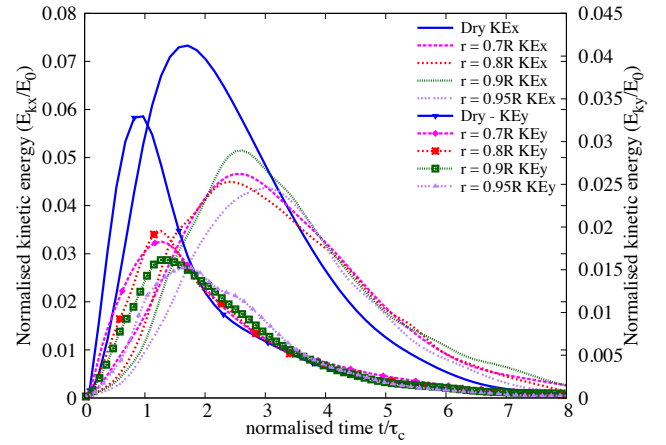
R . As the quantity of material destabilised is small, the flow is thinner and thus has a high Froude's number (0.59). Figure 13b shows that the peak horizontal kinetic velocity observed in the case of $r = 0.9 R$ is higher than $r = 0.95 R$. A Froude's number of 0.59 for $r = 0.9 R$ is observed in contrast to 0.46 for $r = 0.95 R$. Both values of hydrodynamic radii result in a Froude's number that indicate the occurrence of hydroplaning. However, the difference in the amount of material destabilised for $r = 0.95 R$ and the decreased effect of hydroplaning results in a shorter run-out distance for $r = 0.95 R$ in comparison to $r = 0.9 R$.

Figure 14a shows the evolution of packing fraction with time for different values of permeability. As the column collapses, water is entrained at the flow front. This can be observed by the decrease in the packing fraction during $t = \tau_c$ and $t = 3\tau_c$. As the flow progresses, the entrained water is expelled and the soil grains consolidate to reach a critical packing density at the end of the flow. The permeability (i.e., hydrodynamic radius) plays a crucial role in the rate of dissipation of the entrained water. As the permeability decreases, the water entrained at the flow front takes longer time to be dissipated resulting in lubrication of the flow at low permeabilities. Figure 14b shows that the low permeable columns exhibit higher Froude's numbers, greater than 0.4, that indicates occurrence of hydroplaning. This lubrication effect results in an increase in the run-out distance for columns with low permeabilities.

The evolution of grain trajectories with time are presented in figure 15 for low ($r = 0.95 R$) and high ($r = 0.9 R$) permeability conditions. It can be observed that a high permeability column shows a parabolic (convex) final profile in contrast to the more concave profile observed in low permeability condition, due to the effect of drag forces on the flow front. This difference in the flow thickness results in a higher value of Froude's number (0.59) and the occurrence of hydroplaning in the low permeability condition. Due to the high permeability, the water entrained at the flow front is dissipated quicker and thus no lubrication effect is observed. A Froude's number of 0.272 (no hydroplaning) is observed for the high permeability con-

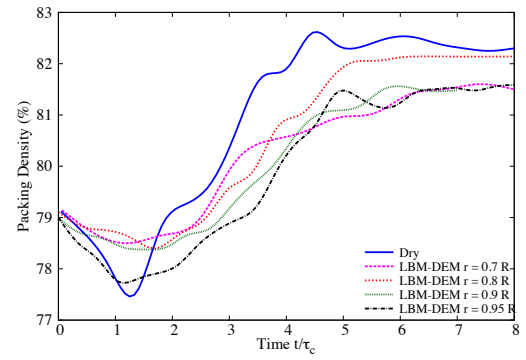


(a) Evolution of the total kinetic energy.

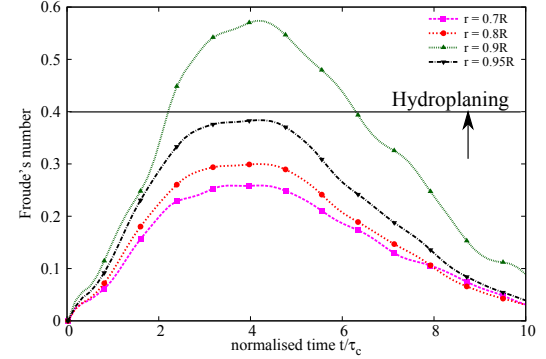


(b) Evolution of horizontal and vertical kinetic energies.

Figure 13: Effect of permeability on the evolution of kinetic energies with time for a granular column collapse in fluid ($a = 0.8$ & loose packing).

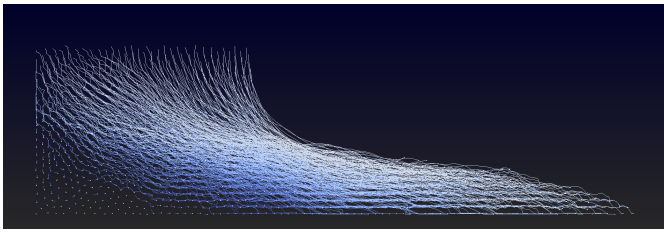


(a) Evolution of packing density.

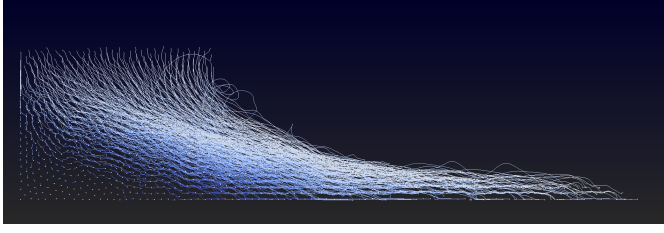


(b) Evolution of Froude's number.

Figure 14: Effect of permeability on the evolution of packing density and Froude's number for a granular column collapse in fluid ($a = 0.8$ & loose initial packing).



(a) High permeability ($r = 0.7 R$).



(b) Low permeability ($r = 0.95 R$).

Figure 15: Particle tracking of the deposit morphology for a granular column collapse in fluid ($a = 0.8$ & loose packing), influence of permeability.

dition ($r = 0.7 R$). The thick flow front in dense condition results in higher effective stress, in contrast to the low effective stress in loose condition due to positive pore-pressure at the flow front. The higher effective stress results in more frictional dissipation in dense condition, while the loose column experiences lubrication effect. This shows that the drag force predominates at high permeability, while the low permeability condition is characterised by hydroplaning and lubrication.

Figure 16 shows the normalised pressure at the base for the low and high permeability flows at $t = 2\tau_c$. The normalised effective stress plotted is obtained as the average over 5 time steps at $2\tau_c$. The effective stress at the base is normalised to the effective stress of a static granular column before the collapse. A value of 1 indicates that the effective stress hasn't changed, which can be observed in the static region of the granular column. It can be observed that the normalised effective stress is significantly higher for the high permeability condition at the flow front in comparison to the almost non-existence of effective stress in the low permeability condition. The observation of trivial effective stress at the flow front corroborates the lubrication effect observed at low permeability conditions.

Figure 18 shows the grain trajectories of a dense and a loose initial packing for a hydrodynamic radius ($r = 0.95 R$). It can be observed that the dense initial packing results in a lot of turbulent behaviour at the flow surface in contrast to the more uniform flow behaviour in the loose condition. The thickness of the deposit in both dense and loose condition is almost the same, however the density of the flow results in a Froude's number of 0.59 and 0.429 for loose and dense conditions, respectively. The low initial density results in more hydroplaning in the loose condition. The effect of water entrainment at the flow front in dense and loose conditions can be seen in figure 17. Water entrainment at the flow front can be observed in the loose condition, this is shown by white-coloured

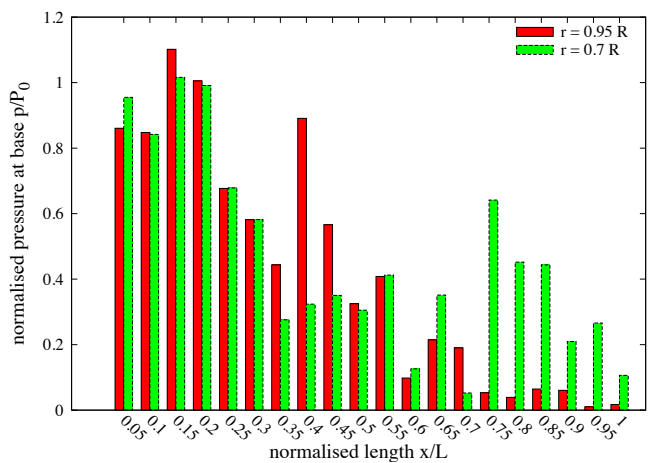


Figure 16: Effect of permeability on the normalised effective stress for loose initial packing at $t = 2\tau_c$.

(empty Voronoi cells) at the flow front. This empty region in the granular packing between the granular mass and the base at the flow front represents the entrained water, which results in hydroplaning. Comparing the evolution packing densities in dense and loose conditions (figures 8a and 14a) reveal almost the same packing density when the flow is fully mobilised. Hence, it is the density of the flowing granular mass that controls the influence of hydroplaning for a given hydrodynamic radius and initial aspect ratio. A loosely packed granular column with low permeability entrains more water at the flow front, resulting in a hydroplaning effect that overcomes the influence of viscous drag forces and thereby yields a higher run-out distance than the dry condition.

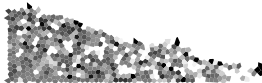
5 SUMMARY

Two-dimensional LB-DEM simulations were performed to understand the behaviour of submarine granular flows. Unlike dry granular collapse, the run-out behaviour in fluid is dictated by the initial volume fraction. Rondon, Pouliquen, & Aussillous 2011 also observed that the collapse of a granular column in a viscous fluid is mainly controlled by the initial volume fraction and not by the aspect ratio of the column. The role of the initial volume fraction observed explains the pore pressure feedback mechanism proposed by Schaeffer & Iverson 2008, Iverson 2000 in the context of landslides. The compaction or dilation of grains can cause additional stress in the grains which can stabilise or destabilise the soil. The flow is thus controlled by the coupling between the dilatancy of the granular layer and the development of pore pressure in the fluid phase (Pailha, Pouliquen, & Nicolas 2008). The dense column needs to dilate in order to flow. When it starts to fall, liquid is then sucked into the column, which is then stabilised by the additional viscous drag (Rondon, Pouliquen, & Aussillous 2011, Topin, Monerie, Perales, & Radjaï 2012). By opposition the loose column when it starts flowing expands and ejects liquid, leading to a partial

fluidisation of the material.

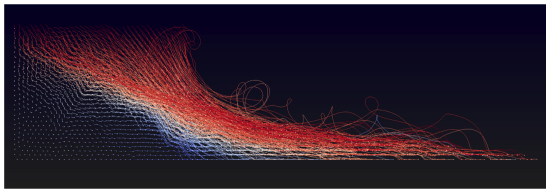


(a) Dense initial packing (83%)

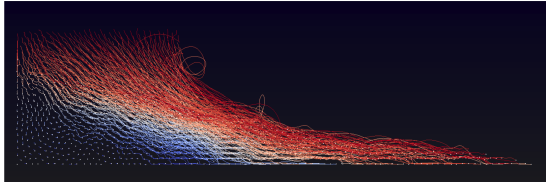


(b) Loose initial packing (79%)

Figure 17: Evolution of packing fraction at $t = \tau_c$ for dense and loose initial packing fraction. Black means dense packing, while white colour denotes loose packing in the Voronoi cell.



(a) Dense initial packing (83%)



(b) Loose initial packing (79%)

Figure 18: Effect of initial density on the deposit morphology for a granular column collapse in fluid ($a = 0.8$). Dense vs. loose initial packing fraction ($r = 0.95 R$). Darker means dense packing, white indicates loose packing density.

- Peker, S. & S. Helvacı (2007). *Solid-liquid two phase flow*. Elsevier.
- Rondon, L., O. Pouliquen, & P. Aussillous (2011, jul). Granular collapse in a fluid: Role of the initial volume fraction. *Physics of Fluids* 23(7), 073301–073301–7.
- Schaeffer, D. G. & R. M. Iverson (2008, jan). Steady and Intermittent Slipping in a Model of Landslide Motion Regulated by Pore-Pressure Feedback. *SIAM Journal on Applied Mathematics* 69(3), 769–786.
- Smagorinsky, J. (1963). General circulation experiments with the primitive equations. *Monthly weather review* 91(3), 99–164.
- Succi, S. (2001). *The lattice Boltzmann equation for fluid dynamics and beyond*. Oxford University Press.
- Topin, V., F. Dubois, Y. Monerie, F. Perales, & A. Wachs (2011). Micro-rheology of dense particulate flows: Application to immersed avalanches. *Journal of Non-Newtonian Fluid Mechanics* 166(1-2), 63–72.
- Topin, V., Y. Monerie, F. Perales, & F. Radjaï (2012, nov). Collapse Dynamics and Runout of Dense Granular Materials in a Fluid. *Physical Review Letters* 109(18), 188001.
- Yu, H., S. Girimaji, & L. Luo (2005). Lattice Boltzmann simulations of decaying homogeneous isotropic turbulence. *Physical Review E* 71(1), 016708.

REFERENCES

- Cook, B., D. Noble, & J. Williams (2004). A direct simulation method for particle-fluid systems. *Engineering Computations* 21(2/3/4), 151–168.
- Denlinger, R. & R. Iverson (2001). Flow of variably fluidized granular masses across three-dimensional terrain, ii: Numerical predictions and experimental tests. *J. Geophys. Res.* 106(B1), 553–566.
- Du, R., B. Shi, & X. Chen (2006, dec). Multi-relaxation-time lattice Boltzmann model for incompressible flow. *Physics Letters A* 359(6), 564–572.
- He, X., Q. Zou, L. S. Luo, & M. Dembo (1997). Analytic solutions of simple flows and analysis of nonslip boundary conditions for the lattice Boltzmann BGK model. *Journal of Statistical Physics* 87(1), 115–136.
- Iverson, R. M. (2000). Acute Sensitivity of Landslide Rates to Initial Soil Porosity. *Science* 290(5491), 513–516.
- Liu, S. H., D. A. Sun, & Y. Wang (2003). Numerical study of soil collapse behavior by discrete element modelling. *Computers and Geotechnics* 30(Compindex), 399–408.
- Meruane, C., A. Tamburino, & O. Roche (2010). On the role of the ambient fluid on gravitational granular flow dynamics. *Journal of Fluid Mechanics* 648, 381–404.
- Pailha, M., O. Pouliquen, & M. Nicolas (2008). Initiation of Submarine Granular Avalanches: Role of the Initial Volume Fraction. *AIP Conference Proceedings* 1027(1), 935–937.